THE JOURNAL OF PHYSICAL CHEMISTRY A LETTERS

2006, *110,* 3352−3355
Published on Web 02/18/2006

Mixed Frequency/Time Domain Optical Analogues of Heteronuclear Multidimensional NMR

Andrei V. Pakoulev,[†] Mark A. Rickard,[†] Kent A. Meyer,[§] Kathryn Kornau,[†] Nathan A. Mathew,[†] David E. Thompson,[‡] and John C. Wright*,[†]

Department of Chemistry, University of Wisconsin, Madison, Wisconsin 53706, and Department of Chemistry, Lawrence University, Appleton, Wisconsin 54912

Received: December 15, 2005; In Final Form: February 7, 2006

Ultrafast spectroscopy is dominated by time domain methods such as pump−probe and, more recently, 2D-IR spectroscopies. In this paper, we demonstrate that a mixed frequency/time domain ultrafast four wave mixing (FWM) approach not only provides similar capabilities, but it also provides optical analogues of multiple- and zero-quantum heteronuclear nuclear magnetic resonance (NMR). The method requires phase coherence between the excitation pulses only over the dephasing time of the coherences. It uses twelve coherence pathways that include four with populations, four with zero-quantum coherences, and four with double-quantum coherences. Each pathway provides different capabilities. The population pathways correspond to those of two-dimensional (2D) time domain spectroscopies, while the double- and zero-quantum coherence pathways access the coherent dynamics of coupled quantum states. The three spectral and two temporal dimensions enable the isolation and characterization of the spectral correlations between different vibrational and/or electronic states, coherence and population relaxation rates, and coupling strengths. Quantum-level interference between the direct and free-induction decay components gives a spectral resolution that exceeds that of the excitation pulses. Appropriate parameter choices allow isolation of individual coherence pathways. The mixed frequency/time domain approach allows one to access any set of quantum states with coherent multidimensional spectroscopy.

The recent development of coherent two-dimensional vibrational spectroscopy has provided a complementary approach to incoherent pump−probe spectroscopy. The 2D-IR methods are the optical analogues of multidimensional NMR, and they are now feasible using both frequency and time domain nonlinear four wave mixing (FWM) methods.[1−14] Time domain 2D-IR methods measure the temporal oscillation of the nonlinear coherences, while frequency domain methods measure the FWM intensity while scanning the excitation pulse frequency. There is interest in developing the optical analogues of heteronuclear NMR where one can establish multiple- and zero-quantum (MQ−ZQ) coherences between any quantum states.[4,7,15] For example, Scheurer and Mukamel[15] have proposed the heteronuclear three-pulse coherence transfer (CT3) and the modified heteronuclear multiple-quantum coherence schemes (HMQC′) as practical NMR analogues. The MQ−ZQ coherences form networks of coupled states that simplify complex spectra and establish the correlations required for obtaining structural and dynamical details about a sample.[16,17] MQ−ZQ methods require phase coherence between the excitation pulses. Time domain methods require long-term phase coherence throughout the measurement of the temporal oscillations. Long-term phase coherence is easily achieved in NMR[16,17] but difficult at the higher frequencies required for optical analogues. Currently, phase coherence is achieved by deriving the excitation pulses from a single pulse with sufficient bandwidth to excite the quantum states of interest,[18] but this approach is limited to quantum states which fall within the achievable bandwidth. It is important for multidimensional optical methods to access quantum states with arbitrary energy differences.

In this paper, we demonstrate that mixed frequency/time domain spectroscopies avoid the requirement for long-term phase coherence, since phase coherence is only required during the dephasing time.[19] We present all of the possible four wave mixing (FWM) analogues of heteronuclear NMR methods, including the CT3 and HMQC′ methods proposed recently by Scheurer and Mukamel.[15] We show that the mixed frequency/time domain approach provides the same spectral resolution and dynamic measurement capability as time domain methods, and it allows one to apply coherent multidimensional spectroscopy to the wide range of quantum states of interest in science. We also show that the spectral resolution can be enhanced by increasing the delays between the excitation pulses.

The mixed frequency/time domain analogues also provide a coherent generalization of ultrafast pump−probe methods. Here, three excitation pulses entangle different coupled quantum states. One pumps either a population or a MQ−ZQ coherence with the first two pulses and probes their time evolution with a third pulse. Rather than sensing the changes in the probe intensity, one measures the intensity of a new beam as a function of the

[†] University of Wisconsin.
[‡] Lawrence University.
[§] Current address: Oak Ridge National Laboratories, P.O. Box 2008, Oak Ridge, Tennessee 37831.

10.1021/jp057339y CCC: $33.50

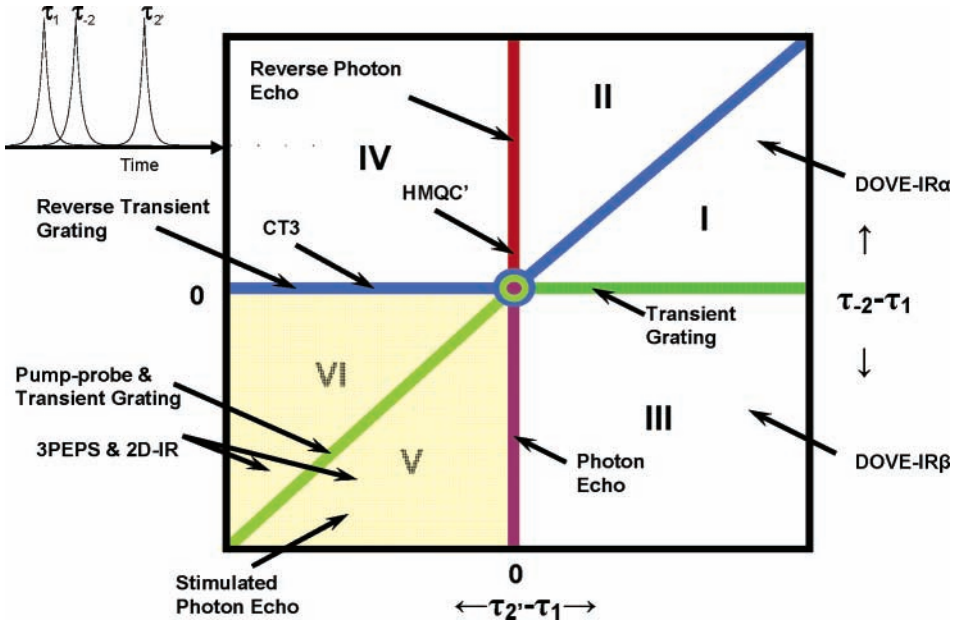

Figure 1. The diagram categorizes the different time orderings of three excitation pulses for the $\vec{k}_4 = \vec{k}_1 - \vec{k}_{-2} + \vec{k}_{2'}$ phase matching condition. The excitation frequencies (ω_1, ω_2, ω_2') may be equal or different. Each time ordering corresponds to different coherence pathways, and these pathways are shown as part of Figure 3. The *x* and *y* axes are $\tau_2' - \tau_1$ and $\tau_{-2} - \tau_1$, respectively, and zero delay is in the center. Example pulses are shown for positive time orderings of $\tau_2' - \tau_1$ and $\tau_{-2} - \tau_1$. The different regions are labeled using the previously published conventions.[30] The time orderings for other FWM mixing processes are also indicated to allow comparison.

frequencies and pulse delays. The state populations reflect the incoherent dynamics, while the MQ−ZQ coherences reflect the coherent dynamics. The three spectral and two temporal dimensions in this method allow isolation of particular coherence pathways and resolve the bleaching, stimulated emission, and excited-state absorption pathways that complicate pump−probe experiments.[20]

The experiment uses three picosecond infrared pulses (labeled 1, −2, 2′) with frequencies ω_1 and ω_2, pulse delays $\tau_{2'} - \tau_1$ and $\tau_{-2} - \tau_1$, and phase-matching $\vec{k}_4 = \vec{k}_1 - \vec{k}_{-2} + \vec{k}_{2'}$. A monochromator at ω_m spectrally resolves the nonlinear signal. The first pulse excites a coherence, the second pulse excites either a population or a MQ−ZQ coherence, and the third pulse excites a second coherence. If there is inhomogeneous broadening, the second coherence can result in rephasing or nonrephasing of the nonlinear polarization created by the first pulse. The experiments provide two-dimensional cross-sections of the 5D variable space (ω_1, ω_2, ω_m, $\tau_{-2} - \tau_1$, $\tau_{2'} - \tau_1$) where two variables are scanned and the other variables are fixed. Since the signal contains both a driven and a free induction decay (FID) component, we either fix ω_m at the frequency of the output coherence to optimize the FID component or scan ω_m, so $\omega_m = \omega_1$ to optimize the driven component at $\omega_4 = \omega_1 - \omega_2 + \omega_{2'}$. The sample is a 200-$\mu$m-thick mixture of 10 mM bis(triphenylphosphine)dicarbonyl nickel, $(Ni(CO)_2(PPh_3)_2$, and (triphenylphosphine)tricarbonyl nickel, $(Ni(CO)_3(PPh_3)$, in benzene, which we use as a simple model system to demonstrate the methodology.[21]

Just as NMR uses many different pulse sequences to obtain specific information about particular coherences, each FWM pulse sequence probes three of the five possible FWM coherences and two possible populations. Figure 1 shows the six possible time orderings (labeled I−VI) of FWM.[22] For each time ordering, there is a parametric and nonparametric pathway (labeled α and β). It also shows the time orderings for the familiar photon echo, transient grating, and pump−probe methods,[23] as well as the less familiar reverse photon echo and reverse transient grating methods[5] and the proposed CT3 and

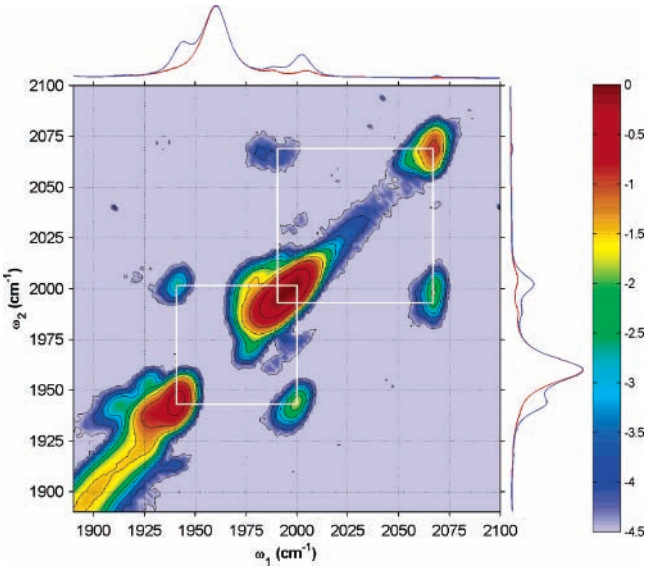

Figure 2. 2D spectrum showing the log(FWM intensity) vs the two excitation frequencies. The lower box indicates the transitions for the $Ni(CO)_2(PPh_3)_2$, and the upper box indicates those for the $Ni(CO)_3PPh_3$. The 1D infrared spectrum of the mixture (blue) and the benzene solvent (red) appears on the top and right side for comparison. The strongest feature at 1962 cm^{-1} is the benzene solvent. The very weak wings on the lower-energy diagonal features are attributed to higher-order processes.

HMQC′ NMR analogues.[15] The time orderings labeled V and VI generate populations that are used extensively to define the incoherent dynamics,[5] while the I−IV time orderings define the coherent dynamics. Time orderings I and III excite zero-quantum coherences with natural line narrowing, and time orderings II and IV excite double-quantum coherences that access two-photon states.[16,17]

Figure 2 shows the ω_1/ω_2 spectrum for time-ordering I where $\omega_m = \omega_1$, $\tau_{2'} - \tau_1 = 2.5$ ps, and $\tau_{-2} - \tau_1 = 1.5$ ps. The Iα,β pathways have zero-quantum coherences that create cross-peaks between different vibrational states that are analogues of those

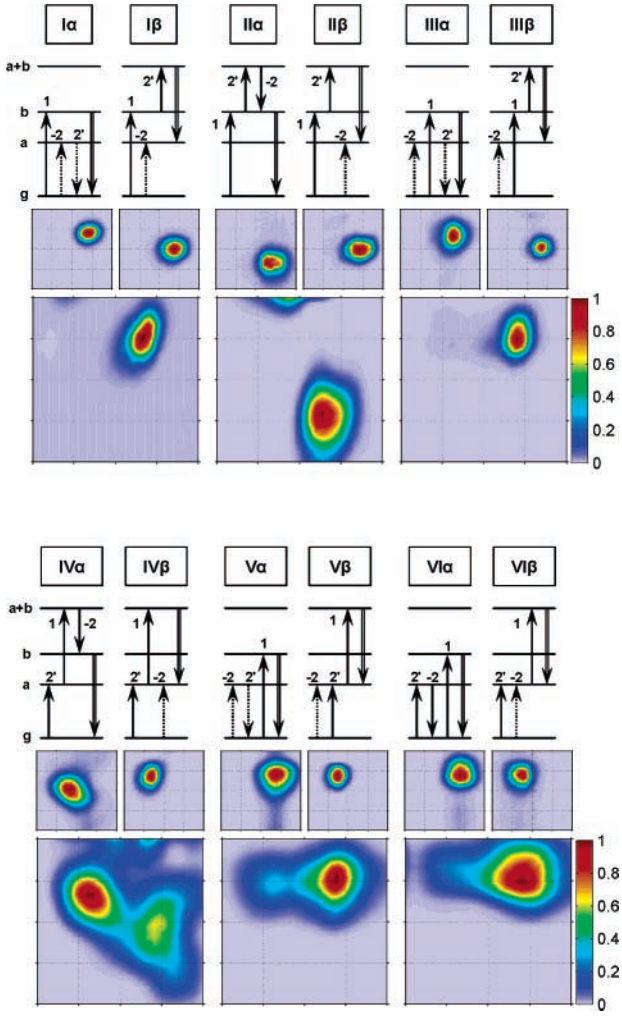

Figure 3. The top row in each sequence shows the WMEL diagrams for the 12 different coherence pathways. The horizontal lines indicate quantum-state energies, and the solid and dotted vertical arrows represent ket and bra side transitions of a coherence. The double arrow represents the output transition. The two rows of spectra show the region of Figure 2 from $(x, y) = (\omega_1, \omega_2) = (1960, 1900)$ to $(2020, 1960)$ cm^{-1} for each coherence pathway with the monochromator set to either 2002 or 1976 cm^{-1} to optimize the FID of the α or β pathways (middle row of spectra) or scanned so $\omega_m = \omega_1$ to optimize the driven signal (bottom row of spectra).

in heteronuclear NMR. The boxes define the diagonal and cross-peaks between the carbonyl stretch modes of the $Ni(CO)_2(PPh_3)_2$ (lower left box) and $Ni(CO)_3(PPh_3)$ (upper right box). The infrared spectrum of this sample is shown on the same scales for comparison.

Figure 2 contrasts markedly with an earlier spectrum[21] taken without time delays or a monochromator so twelve different coherence pathways contribute simultaneously (see Figures 1 and 3). The spectrum in Figure 2 is much sharper, and the features are well-resolved. In fact, the cross-peaks are narrower than the excitation spectral widths.

The spectrum changes for different τ_{-2} and $\tau_{2'}$ time orderings. An example $Ni(CO)_2(PPh_3)_2$ cross-peak is shown in Figure 3 (bottom part) along with the corresponding wave mixing energy level (WMEL) diagrams (top part) for all twelve pathways.[23] The top row of spectra fixes ω_m at the FID output frequency of the α or β pathways, while the bottom row of spectra makes $\omega_m = \omega_1$ so the driven signal from both pathways will be seen. The former condition isolates a particular pathway, while the latter condition isolates a particular time ordering.

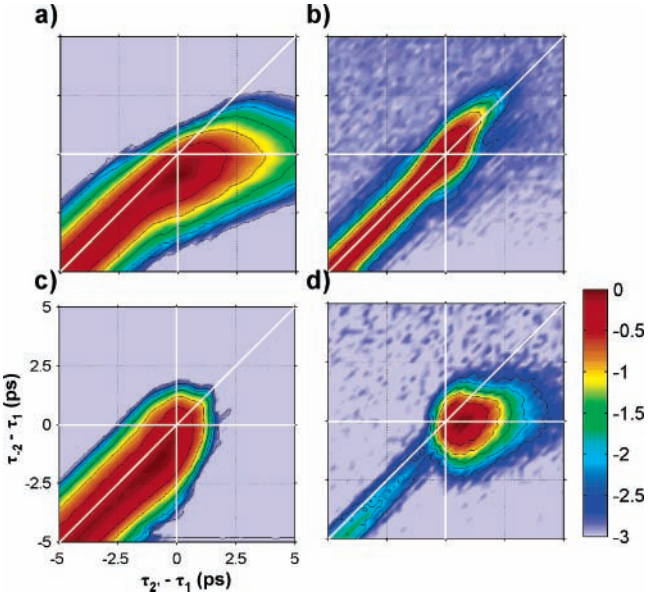

Figure 4. The log(FWM intensity) as a function of the $\tau_{2'} - \tau_1$ (x axis) and $\tau_{-2} - \tau_1$ (y axis) time delays. The excitation frequencies and monochromator position are set to $(\omega_1, \omega_2, \omega_m)$ = (a) (2002, 1943, 2002); (b) (2002, 1917, 2002); (c) (1976, 1943, 1976); and (d) (2002, 1931, 1976) cm^{-1} to optimize the pathways (Iα, IIIα, Vα, VIα), (IIα), (IVβ, Vβ, VIβ), and (Iβ, IIβ, IIIβ), respectively. (The $\omega_2 = 1931$ cm^{-1} setting for 4d optimizes the spectral overlap with fundamental and combination band transitions at 1943 and 1917 cm^{-1}.) The intensities in each region should be compared to Figure 1 in order to see the relative intensities and decay rates for the coherence pathways chosen by each $(\omega_1, \omega_2, \omega_m)$ combination.

The cross-peak position in Figure 3 depends on a pathway's coherences and the experimental parameters. The four states (labeled g, a, b, and (a + b)) form five coherences labeled bg, ag, ba, (a + b)g, and (a + b)a. The $Ni(CO)_2(PPh_3)_2$ coherences in the twelve pathways are resonantly enhanced when the excitation frequencies are respectively set to $\omega_1 = 2002$, $\omega_2 = 1943$, $\omega_1 - \omega_2 = 59$, $\omega_1 + \omega_2 = 3919$, and $\omega_1 - \omega_2 + \omega_{2'} = 1976$ cm^{-1} and these conditions define the cross-peak positions. For example, pathway Iα involves bg, ba, and bg coherences, so the cross-peak appears at $(\omega_1 = 2002, \omega_2 = 1943)$ cm^{-1}. Pathway IVβ involves ag, (a + b)g, and (a + b)a coherences, so the cross-peak appears at $(\omega_2 = 1943, \omega_1 = 1976)$ cm^{-1}. In both examples, the pathways can be fully resonant with the two excitation frequencies, and the cross-peaks appear at the expected positions. Similar arguments correctly predict the cross-peak positions for the other six fully resonant pathways, for spectra with ω_m both fixed and scanned. Pathways Iβ, IIβ, IIIβ, and IVα cannot be fully resonant if $\omega_2 = \omega_{2'}$. Their cross-peak appears at frequencies where the excitation pulse bandwidth optimizes the three resonances.

With the delay times used for these experiments, the cross-peaks are spectrally narrower than the excitation pulses that create them. Shorter delay times lead to broader cross-peaks. This narrowing is predicted by simulations that account for the Gaussian frequency distribution of the excitation pulses. The narrowing results from interference between the driven and FID components during the pulses which effectively extends the measurement time.

The dynamics can be measured by changing the delay times. Figure 4 shows two-dimensional representations of the $\tau_{2'} - \tau_1$ and $\tau_{-2} - \tau_1$ dependence for representative values of ω_1, ω_2, and ω_m. It is the experimental implementation of Figure 1, and it contains all of the dynamical information about populations and coherences. For this paper, the figure shows how the

intensities change when different pathways are chosen by the different time delays. In Figure 4a, for example, setting $\omega_1 = 2002$, $\omega_2 = 1943$, $\omega_m = 2002$ cm^{-1} allows triply resonant contributions from pathways Iα, IIIα, Vα, and VIα, and the corresponding regions in the figure have large intensities. The finite duration of the excitation pulse results in some contribution in regions II and IV. If one selects a point in region I and moves horizontally to more positive $\tau_{2'} - \tau_1$ values, the decay defines the dephasing rate of the ba coherence, Γ_{ba}. If one moves diagonally to more positive values of $\tau_{2'} - \tau_1$ and $\tau_{-2} - \tau_1$, the decay defines Γ_{bg}. Moving diagonally to more negative values of $\tau_{2'} - \tau_1$ and $\tau_{-2} - \tau_1$ in regions V or VI defines the population relaxation, Γ_{gg}.

If one selects different values for ω_1, ω_2, and ω_m, different pathways are optimized, and the shapes of the temporal dependences change depending on which pathways are enhanced by the specific (ω_1, ω_2, ω_m) values. Figure 4b,c,d corresponds to ω_1, ω_2, and ω_m values that optimize the IIα; IVβ, Vβ, and VIβ; and Iβ, IIβ, and IIIβ pathways, respectively. Comparison of Figure 4a−d provides an overdetermined measurement of the system dynamics. It reveals that, in addition to the dephasing kinetics, rephasing of the inhomogeneous broadening, coherence transfer, and quantum beating effects are important in quantitatively describing the dynamics in Figure 4. A quantitative description of these effects is beyond the scope of this letter and will be described in a later publication.

The different pathways have different spectral characteristics.[22] The correlations between the first and third coherences in time orderings III and V provide rephasing and inhomogeneous line narrowing when broadening produces correlated shifts, while those in pathways IV and VI provide rephasing and line narrowing for anticorrelated broadening. The second coherence in time orderings I and III are zero-quantum coherences that exhibit natural line narrowing[22] for correlated broadening, while II and IV create double-quantum coherences where the broadening effects are amplified for correlated broadening.[16,17] The effects are reversed for anticorrelated broadening. Time orderings V and VI create populations that correlate with traditional pump−probe methods and the time domain multidimensional spectroscopies. Appropriate choice of the different pathways allows one to measure the spectra and dynamics of all the coherences.

The feasibility of the mixed frequency/time domain analogue to heteronuclear NMR opens new measurement opportunities. Although this work used vibrational levels to define the characteristics of the approach, the methods are universal and apply equally to electronic and/or vibrational states. For example, earlier work with triply resonant multidimensional spectroscopy accessed coupled vibronic and electronic states,[24−27] while doubly vibrationally enhanced (DOVE) FWM used time orderings I and III with a virtual electronic state and two vibrational states.[1,28] The twelve pathways represent all possible FWM analogues to heteronuclear NMR. The multiple dimensions provide flexibility in extracting spectral and dynamic information. For example, isolation of a specific coherence pathway avoids the ambiguities of the bleaching, stimulated emission, and excited-state absorption pathways in pump−probe methods, and it resolves the effects of spectral diffusion and relaxation.[20] One can also isolate the coherent or incoherent dynamics and determine the correlations between different quantum states. The use of the mixed frequency/time domain methods also opens opportunities for more sophisticated methods. Higher-order nonlinear mixing processes allow one to access higher-order coherences that provide greater simplification and more information about the correlation of quantum states. All of these methods are capable of multidimensional imaging analogous to the one-dimensional imaging of coherent anti-Stokes Raman spectroscopy (CARS).[29] If both infrared and UV/visible pulses were used, one could have the selectivity of a vibrational measurement and the spatial resolution of a UV/visible pulse.

Acknowledgment. This work was supported by the Chemistry Division of the National Science Foundation under grant CHE0130947.

References and Notes

(1) Zhao, W.; Wright, J. C. *Phys. Rev. Lett.* **1999**, *83*, 1950.
(2) Zhao, W.; Wright, J. C. *Phys. Rev. Lett.* **2000**, *84*, 1411.
(3) Wright, J. C.; Zhao, W.; Murdoch, K. M.; Besemann, D. M.; Condon, N. J.; Meyer, K. A. Nonlinear 2D Vibrational Spectroscopy. In *Handbook of Vibrational Spectroscopy*; Chambers, J. M., Griffiths, P. R., Eds.; John Wiley and Sons: New York, 2001.
(4) Keusters, D.; Tan, H. S.; Warren, W. S. *J. Phys. Chem. A* **1999**, *103*, 10369.
(5) Mukamel, S. *Annu. Rev. Phys. Chem.* **2000**, *51*, 691.
(6) Warren, W.; Zewail, A. H. *J. Chem. Phys.* **1983**, *78*, 2279.
(7) Tian, P. F.; Keusters, D.; Suzaki, Y.; Warren, W. S. *Science* **2003**, *300*, 1553.
(8) Hamm, P.; Lim, M.; DeGrado, W. F.; Hochstrasser, R. M. *Proc. Natl. Acad. Sci. U.S.A.* **1999**, *96*, 2036.
(9) Asplund, M. C.; Zanni, M. T.; Hochstrasser, R. M. *Proc. Natl. Acad. Sci. U.S.A.* **2000**, *97*, 8219.
(10) Hybl, J. D.; Albrecht, A. W.; Faeder, S. M. G.; Jonas, D. M. *Chem. Phys. Lett.* **1998**, *297*, 307.
(11) Hybl, J. D.; Ferro, A. A. A.; Jonas, D. M. *J. Chem. Phys.* **2001**, *115*, 6606.
(12) Brixner, T.; Stenger, J.; Vaswani, H. M.; Cho, M.; Blankenship, R. E.; Fleming, G. R. *Nature (London)* **2005**, *434*, 625.
(13) Cowan, M. L.; Bruner, B. D.; Huse, N.; Dwyer, J. R.; Chugh, B.; Nibbering, E. T. J.; Elsaesser, T.; Miller, R. J. D. *Nature (London)* **2005**, *434*, 199.
(14) Golonzka, O.; Khalil, M.; Demirdoven, N.; Tokmakoff, A. *Phys. Rev. Lett.* **2001**, *86*, 2154.
(15) Scheurer, C.; Mukamel, S. *J. Chem. Phys.* **2002**, *116*, 6803.
(16) Munowitz, M.; Pines, A. Pinciples and Applications of Multiple-Quantum NMR. In *Advances in Chemical Physics*; Prigoginie, I., Rice, S. A., Eds.; John Wiley and Sons: New York, 1987; Vol. LXVI; p 1.
(17) Munowitz, M.; Pines, A. *Science* **1986**, *233*, 525.
(18) Rubtsov, I. V.; Wang, J. P.; Hochstrasser, R. M. *Proc. Natl. Acad. Sci. U.S.A.* **2003**, *100*, 5601.
(19) Cho, M. Two-Dimensional Vibrational Spectroscopy. In *Advances in Multi-Photon Processes and Spectroscopy*, 1st ed.; Lin, S. H., Villaeys, A. A., Fujimura, Y., Eds.; World Scientific: Singapore, 1999; Vol. 12, p 1.
(20) Hamm, P.; Lim, M.; Hochstrasser, R. M. *J. Phys. Chem. B* **1998**, *102*, 6123.
(21) Meyer, K. A.; Wright, J. C. *Chem. Phys. Lett.* **2003**, *381*, 642.
(22) Besemann, D. M.; Meyer, K. A.; Wright, J. C. *J. Phys. Chem. B* **2004**, *108*, 10493.
(23) Wright, J. C. *Int. Rev. Phys. Chem.* **2002**, *21*, 185.
(24) Carlson, R. J.; Nguyen, D. C.; Wright, J. C. *J. Chem. Phys.* **1990**, *92*, 1538.
(25) Carlson, R. J.; Wright, J. C. *J. Chem. Phys.* **1990**, *92*, 5186.
(26) Carlson, R. J.; Wright, J. C. *J. Chem. Phys.* **1990**, *93*, 2205.
(27) Carlson, R. J.; Wright, J. C. *Anal. Chem.* **1991**, *63*, 1449.
(28) Zhao, W.; Wright, J. C. *J. Am. Chem. Soc.* **1999**, *121*, 10994.
(29) Volkmer, A.; Cheng, J. X.; Xie, X. S. *Phys. Rev. Lett.* **2001**, *87*, 3901.
(30) Meyer, K. A.; Thompson, D. E.; Wright, J. C. *J. Phys. Chem. B* **2004**, *108*, 11485.